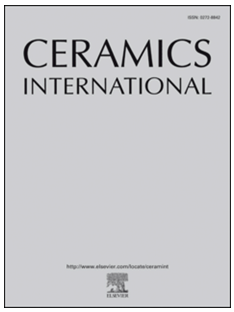

Hierarchical, template-free self-assembly morphologies IN CeO_2 synthesized via urea-hydrothermal method

Rosario Suarez Anzorena, Fernando F. Muñoz, Pablo Bonelli, Ana Lea Cukierman, Susana A. Larrondo

PII: S0272-8842(20)30232-7

DOI: https://doi.org/10.1016/j.ceramint.2020.01.212

Reference: CERI 24144

To appear in: *Ceramics International*

Received Date: 17 November 2019

Revised Date: 23 December 2019

Accepted Date: 23 January 2020

Please cite this article as: R.S. Anzorena, F.F. Muñoz, P. Bonelli, A.L. Cukierman, S.A. Larrondo, Hierarchical, template-free self-assembly morphologies IN CeO_2 synthesized via urea-hydrothermal method, *Ceramics International* (2020), doi: https://doi.org/10.1016/j.ceramint.2020.01.212.

HIERARCHICAL, TEMPLATE-FREE SELF-ASSEMBLY MORPHOLOGIES IN CeO_2 SYNTHESIZED VIA UREA-HYDROTHERMAL METHOD

Rosario Suarez Anzorena[1], Fernando F. Muñoz[1,3], Pablo Bonelli[2,3], Ana Lea Cukierman[2,3,4], Susana A. Larrondo*[1,3,5]

[1]*UNIDEF, CONICET, MINDEF, Departamento de Investigaciones en Sólidos, CITEDEF, J.B. de La Salle 4397, B1603ALO Villa Martelli, Pcia. de Buenos Aires, Argentina.*

[2] *Instituto de Tecnología de Alimentos y Procesos Químicos (ITAPROQ) Consejo Nacional de Investigaciones Científicas y Técnicas (CONICET), Universidad de Buenos Aires, Ciudad Universitaria, Buenos Aires, Argentina.*

[3] *Consejo Nacional de Investigaciones Científicas y Técnicas (CONICET), Godoy Cruz 2290 C1425FQB Buenos Aires, Argentina.*

[4] *Universidad de Buenos Aires, Facultad de Farmacia y Bioquímica, Departamento de Tecnología Farmacéutica, Cátedra de Tecnología Farmacéutica II, Junín 956, C1113AAD Buenos Aires, Argentina.*

[5] *Instituto de Investigación e Ingeniería Ambiental, UNSAM, Campus Miguelete, 25 de Mayo y Francia, 1650 San Martín, Pcia. de Buenos Aires, Argentina.*

**Corresponding Author: slarrondo@citedef.gob.ar; slarrondo@unsam.edu.ar*

Abstract

Nano-crystalline CeO_2 was synthesized via the urea-hydrothermal method without templates or **structure-directing** agents. **The synthesis parameters Ce^{3+} to Ce^{4+} and urea to cation molar ratios, reaction temperature and reaction time were varied to analyze their effect on morphology, texture and reducibility.** The analysis of the obtained morphologies provides strong evidence of a hierarchical and sequential template-free self-assembly process **that evolves** from shuttles to dumbbells to spheres. In all cases, **the** morphology **of samples** remains unchanged even after calcination at 500 °C. The presence of Ce^{4+} in the initial solution clearly provides the full **self-assembly** sequence and **is decisive for obtaining** non-hollow spheres of CeO_2 with high specific surface area and high pore volume. Besides, if only Ce^{3+} is present, typical $CeOHCO_3$ shuttle-like particles **with orthorhombic structure are obtained**. The use of Ce^{3+} in combination with Ce^{4+} **produces partial sequences of the self-assembly process that provide a strong indication of the hierarchical sequence.**

The urea to cation molar ratio controls the nucleation process and proves to be crucial to obtain the self-assembly sequence. On the other hand, temperature and reaction time show a moderate effect on morphology.

Keywords: ceria; hydrothermal synthesis; self-assembly morphologies

Graphical Abstract

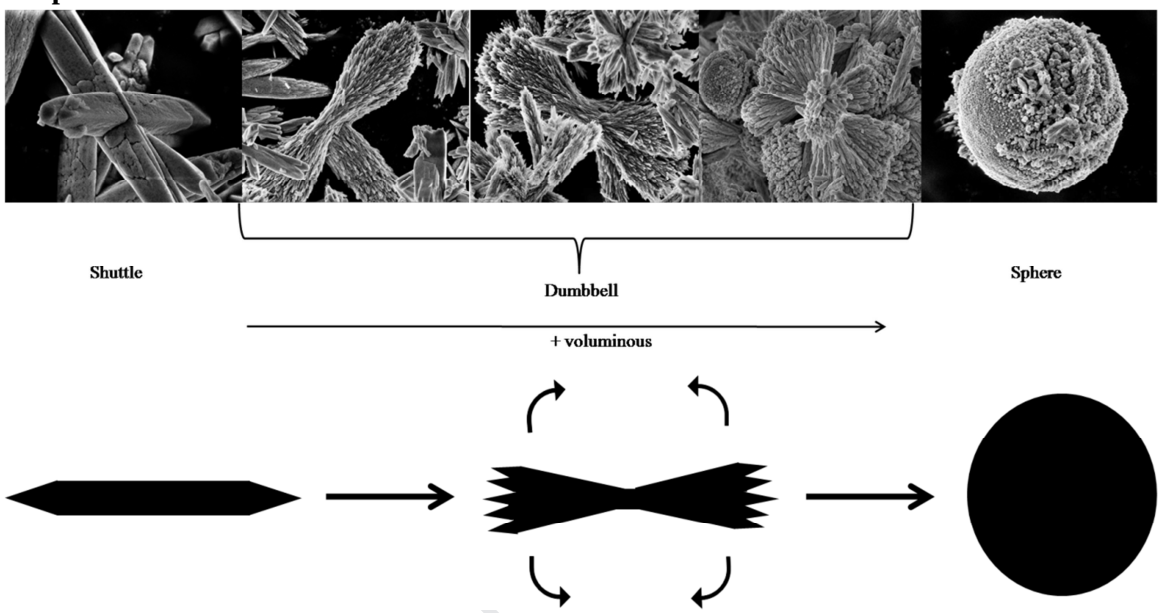

Introduction

CeO_2-based materials have many applications as catalysts, electrocatalysts, electrolytes and electrodes in Solid Oxide Fuel Cell (SOFC), gas sensors, and photocatalysts in the UV-visible region, among other uses [1, 2]. The rapid and reversible inter-conversion between its two oxidation states, Ce^{3+} and Ce^{4+}, gives this oxide the ability to easily exchange oxygen with the surroundings, **which determines its** extraordinary catalytic properties [3]. The great influence of crystal shape and size on redox properties and the outstanding physicochemical properties observed in nanomaterials triggered the development of many synthesis routes and methods to obtain nanosized and nanostructured ceria-based materials. Among them, the hydrothermal method has proved to be a good alternative to obtain samples with controllable morphology and crystallite size. Many studies with different reactants, solvents, reaction temperatures and reaction times were performed **[4–9].**

Regarding the reactants, NaOH and $Ce(NO_3)_3$ were used to obtain nanorods**[10]**, nano-cubes and nanowires **[11]**. However, the elimination of Na^+ ions from the final solids is difficult and the presence of ions on the ceria surface negatively affects the reactivity of the material. In other studies, urea was used to obtain nanorods **[12],** acrylamide to get nano-cubes **[13]**, templates as PVP (polyvinylpyrrolidone) to produce table-like nanostructures, triangular prism-like nanotubes **[14]**, PVP K30 to obtain hierarchical microspheres **[15]**, and PVA (polyvinyl alcohol) to obtain flower-like and pyramidal polycrystalline particles **[16]**. Hierarchical flower-like microspheres of CeO_2 were obtained with N-containing organic compounds after calcination of $CeOHCO_3$ precursors **[17]**. Other researchers reported the use of hexadecyl trimethyl ammonium bromide **(**CTAB) to obtain star-like self-assembled CeO_2 structures formed by nano-rectangular blocks **[18]** or the use of amine surfactants to obtain rod-like and ellipsoid shaped particles **[19]**.

Some studies reported the synthesis of shuttle-like particles using urea and cerium (III) nitrate ($Ce(NO_3)_3$) as reagents **[20, 21]**, observing nanosphere particles as urea to $Ce(NO_3)_3$ molar ratio increases **[22]**. It was **noted** that the solvent used to prepare the initial solution also influences the morphology observed in the final powder **[23, 24]**. Besides, it was reported that different

sources of Ce^{4+} in the initial solution produces variations in crystallinity, crystallite size and specific surface area **[25]**.

Regarding the reaction temperature and the reaction time, the increase of both parameters increases the crystallite size and decreases the specific surface area of CeO_2 **[20, 23, 25]**.

The analysis of all these reports indicates that the combination of the hydrothermal method with templates has proved to be effective to control morphology. However, despite all the work done, there has been no systematic study of template-free hydrothermal synthesis of ceria so far.

The aim of this work is to contribute to this field by systematically examining the main parameters controlling the template-free hydrothermal synthesis of CeO_2 and their effect on morphology, structure, specific surface area, porosity and redox behavior.

2. Experimental

Synthesis process

The reactants used in the synthesis are urea ($CO(NH_2)_2$, Merck 99.5%), Ce(III) nitrate hexahydrate ($Ce(NO_3)_3.6H_2O$, Merck 99%) and ammonium Ce(IV) nitrate ($(NH_4)_2Ce(NO_3)_6$, Merck 99%). Scheme 1 summarizes the main steps of the process.

The reactants were dissolved in distilled water in the appropriate proportion to obtain a solution with the desired urea to Ce^{3+}/Ce^{4+} molar ratio. The solution was stirred for 15 min at room temperature and the pH was measured using pH-indicator strips. **Afterwards,** the solution was poured into a Teflon® lined autoclave reactor with a capacity of 100 ml. In all the experiments 50% of the vessel capacity was filled. The autoclave **reactor was heated to** the selected reaction temperature, **maintaining this temperature for** the reaction time selected for each specific synthesis. The precipitate obtained was collected by centrifugation at 4000 rpm in two steps of 10 min each and dried at 80 °C **for** 4 h. These solids are named “precursors”. These precursors were then calcined at 500 °C for 2h (heating ramp of 10 **°C min^{-1}**). The absence of turbidity after the addition of NaOH pellets in 10 ml of the mother liquor was used to confirm the complete precipitation of cerium cations during the reaction. Additionally, Ehrlich's reagent test was used to confirm the absence of remnant urea in the mother liquor **[26]**.

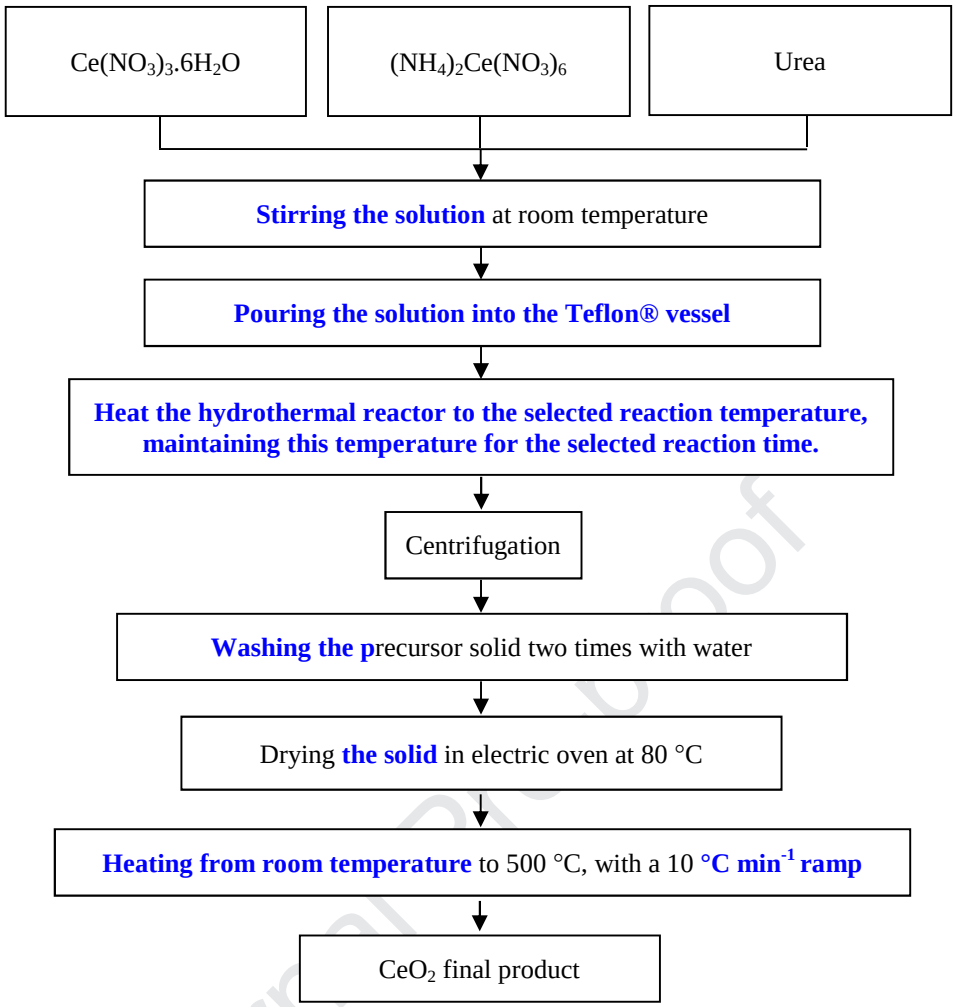

Scheme 1. Main steps of the template-free hydrothermal synthesis of CeO_2.

Four synthesis parameters were varied to analyze their effect on the final solids: **i) Ce^{3+}/Ce^{4+} molar ratio: 0/1, 1/3, 1/1, 1/0; ii) Urea to cation molar ratio (U/C): 0/1, 1/1, 2/1, 4/1;** iii) Reaction Temperature: 100 ºC, 120 ºC, 150 ºC and 180 ºC and iv) Reaction Time: 8h, 16h and 24h. We use structured identifiers to name the samples. As an example, in the name "**CeO_2 U21 C3C411 120 8 500**", **U21** stands for samples with U/C= 2/1, **C3C411** for Ce^{3+}/Ce^{4+}= 1/1, **120** for a reaction temperature of 120 °C, **8** for a reaction time of 8 h and **500** for a calcination temperature of 500 °C. When the sample is not calcined after the drying process the name ends with a **P**, indicating it is a precursor.

Characterization techniques

The crystal structure of the samples was studied by conventional X-ray powder diffraction (XPD) **analysis** performed with a Panalytical Empyrean diffractometer with a PIXCEL3D detector and a Ni filter, operated with Cu-Kα radiation (λ=1,5405980 Å, 40 kV, 40 mA) in the Bragg-Brentano configuration. Data was collected in the 20–100° 2θ range with a time per step of 70 s. Lattice parameters were obtained from Rietveld refinement and compared to the value assumed for pure CeO_2 (a = 0.5413 nm, JCPDS 34-0394). The Williamson-Hall method (WH) **[27]** was used to determine crystallite size (D_v^{WH}) and lattice strain (ε). Microcrystalline LaB_6 was used as **standard** reference material to determine the equipment peak broadening.

Textural characterization was performed by N_2-physisorption isotherm at (−196 °C) determined with an automatic Micromeritics ASAP-2020 HV volumetric sorption analyzer. Prior to gas adsorption measurements, samples were degassed at 120 °C under helium flow for 2 hours. Specific surface areas were determined by applying the standard Brunauer Emmett Teller (BET) procedure. Pore size distributions were obtained from N_2 adsorption isotherm data using the DFT plus software (Micromeritics Instrument Corp) based on nonlocal **Density Functional Theory**.

The morphology of the samples was studied by Scanning Electron Microscopy (SEM, Zeiss Electron Beam SEM-Supra40). SEM images were obtained with the samples placed over an adhesive carbon-filled conductive tape to avoid charging problems. Transmission Electron Microscopy (TEM) analysis was performed with **the** FEI Talos F200a equipment. Samples were dispersed in ethanol by sonication for five minutes. A drop of the solution was transferred **onto** a TEM copper grid coated with a carbon film and **allowed to air dry**.

Hydrogen **temperature-programmed** reduction (H_2-TPR, Micromeritics Chemisorb 2720) was performed to study sample reducibility. The mass employed for each experiment **was 40 mg**. Prior to H_2-TPR tests, samples were pretreated in a 50 **cm^3(STP)min^{-1}** flow of highly pure helium at 300 °C **for** 30 min to remove any adsorbed species on the solid surface. H_2-TPR experiments were carried out with a 50 **cm^3(STP)min^{-1}** flow of 5 vol.% H_2 in argon, from room

temperature up to 900 °C following a heating ramp of 10 **°C min^{-1}**. Hydrogen uptake was estimated using a calibrated Thermal Conductivity Detector (TCD).

Results and discussion

Effect of Ce^{3+} to Ce^{4+} molar ratio in the initial solution

XPD patterns for samples synthesized with different Ce^{3+} to Ce^{4+} molar ratios (Ce^{3+}/Ce^{4+}) show the Bragg peaks corresponding to the fluorite structure of pure CeO_2 (see Figure S1 supplementary information). In Table 1 is possible to see that samples obtained with Ce^{3+}/Ce^{4+} of 0/1 and 1/3 show a smaller lattice parameter than the accepted for pure CeO_2 (0.5413 nm). Regarding the average crystallite size, it is possible to see a clear tendency to lower values as Ce^{3+}/Ce^{4+} decreases. All the values are in the nanometric range.

SEM and TEM results are presented in **Figure 1. Even though the Ce^{3+}/Ce^{4+} ratio has a very mild influence on the crystalline structure, it does have a fundamental influence on the morphology and textural properties.** The micrographs show that the increment of Ce^{4+} concentration in the initial solution produces a well-defined evolution of ordered structures going from shuttles to dumbbells, to almost complete spheres and finally to fully formed spheres. In this succession**,** the preceding morphology is required to achieve the subsequent one [28, 29] (see Scheme 2).

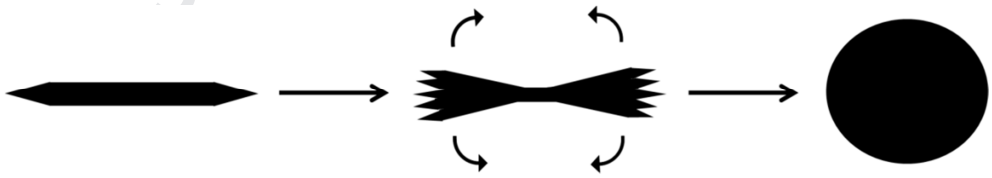

Scheme 2. Schematic representation of the self-assembly sequence.

It is worth to mention that this complete sequence was previously reported, but not for CeO_2 synthesis. In fact, as far as we know, this is the first time that a complete self-assembly growth sequence is observed in CeO_2 synthesis without the use of structure-directing agents, such as organic polymers or surfactants [30, 31]. It can be clearly seen in Figure 1(b) that in the case of equimolar Ce^{3+}/Ce^{4+} molar ratio, only dumbbells and irregular spheres are observed. Besides, in Figure 1(c) referred to Ce^{3+}/Ce^{4+} molar ratio

equal to 1/3, particles very close to regular spheres with a small proportion of dumbbells are observed. In the sample, CeO_2 U21 C3C401 120 8 500 only non-hollow spheres are present with a distribution of sizes in the 100 nm–2 μm range (Figure 1(d)). The obtained results strongly indicate that the complete hierarchical self-assembly sequence is induced by the presence of Ce^{4+}.

It is known that the change in physicochemical properties of water under high-pressure conditions is one of the main characteristics of the hydrothermal method. A very important modification is the decrease in the water dielectric constant **[4],** which has a deep impact in water hydration and ion diffusion capabilities, since a lower dielectric constant means less stabilization for ionic species in solution. Particularly, in our case**,** the dielectric constant value goes from 80 at ambient temperature and pressure, to a value as low as 53 at our experimental conditions.

Scheme 3 presents the nucleation process we propose for **the** Ce^{4+} precursor. When ceric ammonium nitrate is used, the true species in solution is not Ce^{4+} but the complex ion $[Ce(NO_3)_6]^{2-}$ [32], which loses the ligands when the CeO_2 precursor nucleation starts. As shown in **Scheme 3,** since the water in the reaction medium cannot adequately stabilize those NO_3^- anions, they tend to stay near the growing nuclei, keeping them confined in its vicinity. Consequently, the nucleation process develops at a slow rate, in turn providing a very moderate supply of additional cerium to the growth process, thus giving the system the necessary time to complete the entire sequence of self-assembly, which results in fully formed spheres.

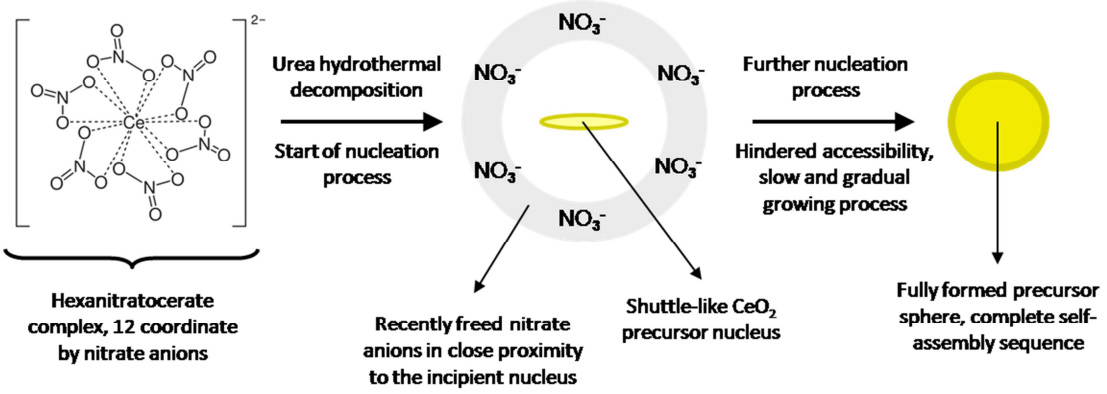

Scheme 3. Proposed nucleation process for Ce^{4+} precursor.

In turn, when only Ce^{3+} is used, which is a **nonahydrate** species **[32, 33]**, the nucleation process involves the loss of only water molecules. Hence, as seen in **Scheme 4**, the growth process occurs at a faster rate since the supply of cerium to the growing nuclei is much more direct, not allowing the full sequence of self-assembly to manifest. As a result, a partial process is observed, with the result of samples with only shuttles and dumbbells morphologies.

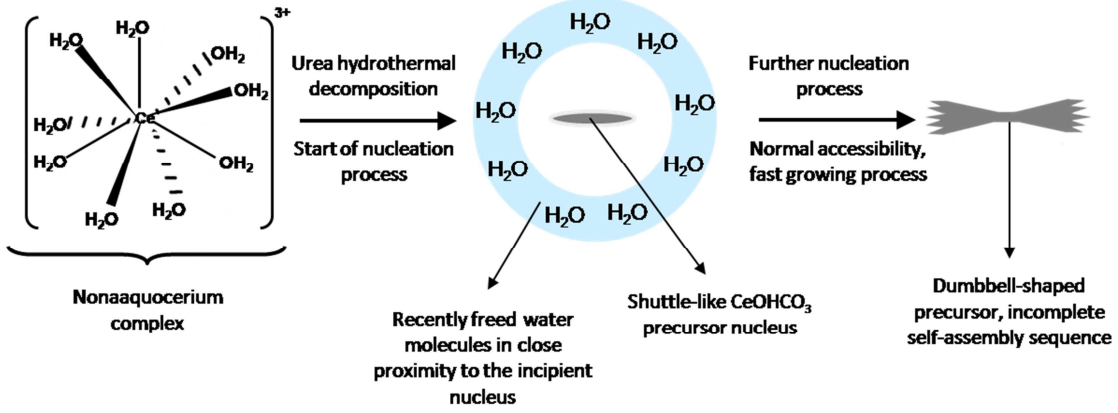

Scheme 4. Proposed nucleation process for Ce^{3+} precursor.

Related to this explanation, the effect of Ce^{4+} can be further examined by analyzing the ionic strength of the solution at the beginning and the end of the synthesis process. These values are presented in Table 2. Since the hydrothermal water has a lower dielectric constant, a reaction medium with increasing ionic strength should be more difficult to stabilize. The values presented in Table 2 indicate that the increase in the content of Ce^{4+} decreases the initial ionic strength. In the case of Ce^{3+}/Ce^{4+} = 0/1, the ionic strength doubles during the reaction. On the contrary, in the Ce^{3+}/Ce^{4+}=1/0 case, the value decreases sharply. The other Ce^{3+}/Ce^{4+} ratios tested show intermediate positive values of ionic strength. These results confirm the nucleation schemes already presented.

XPD patterns of precursors obtained with only Ce^{3+} in the initial solution show the presence of the Bragg peaks of $CeOHCO_3$ orthorhombic structure (Figure S2). As the content of Ce^{4+} increases, it is evident the presence of Bragg peaks corresponding to hexagonal $CeOHCO_3$ and fluorite CeO_2 structures. The precursor obtained using only Ce^{4+} in the initial solution showed only Bragg peaks corresponding to the fluorite-like structure.

Textural properties of the samples are also influenced by the Ce^{3+}/Ce^{4+} molar ratio. In Figure **2** N_2-physisorption isotherms **and pore size distribution** are plotted. The results obtained from the analysis of these isotherms are summarized in Table **1**. Samples synthesized with the presence of Ce^{4+} in the initial solution showed isotherms with shapes **similar to** type IV of IUPAC classification, which is characteristic of mesoporous materials with the presence of micropores in the low-pressure region (Figure **2**). The sample obtained without Ce^{4+} in the initial solution has a markedly low adsorbed volume in the mesopore zone. Specific surface area and total pore volume dramatically increase with the increment of Ce^{4+} concentration in the initial solution, while the percentage of micropore volume drops from 50% to ~25%. **The** pore size distribution **is very symmetrical in all cases and located in the mesoporous range (2–50 nm), with a progressive shift of peak maxima to lower pore sizes as Ce^{4+} concentration increases in the initial solution.**

It is worth to point out the high specific surface area obtained for sample CeO_2 U21 **C3C401** 120 8 500. Similar values were previously reported, like in the case of the reviews by Eastoe et al. **[34, 35]**. **These reviews compiled the highest values of specific surface area so far reported. However, it should be emphasized that these syntheses require complicated procedures and large amounts of organic solvents that constitute an environmental hazard. On the contrary, in the present work, we use no organic solvents and follow a very easy synthesis scheme (see Scheme 1).**

Table 1. Lattice parameters, lattice strain, and crystallite size obtained from Rietveld refinement, total percentage of reduction obtained from H_2-TPR, BET specific surface area, total pore volume, and percentage of micropore volume of samples synthesized with different Ce^{3+}/Ce^{4+} molar ratios in the initial solution.

Sample	a [nm]	ε	D_V^{WH} [nm]	Percentage of Reduction (%)	S_{BET} [$m^2.g^{-1}$]	Total pore Volume [$cm^3.g^{-1}$]	Micropore to Total pore volume (%)
CeO_2 U21 **C3C410**120 8 500	0.5413(7)	$2.1\ 10^{-3}$	15	27	89	0.070	50
CeO_2 U21 **C3C411** 120 8 500	0.5414(0)	$9.0\ 10^{-4}$	10	43	86	0.157	23
CeO_2 U21 **C3C413** 120 8 500	0.5412(6)	$1.1\ 10^{-3}$	8	39	105	0.197	21
CeO_2 U21 **C3C401** 120 8 500	0.5411(2)	$1.5\ 10^{-3}$	6	22	142	0.190	28

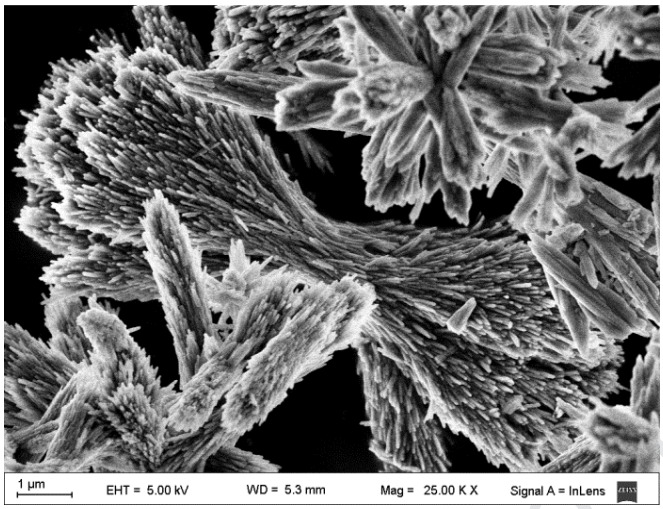

(a) CeO_2 U21 **C3C410** 120 8 500.

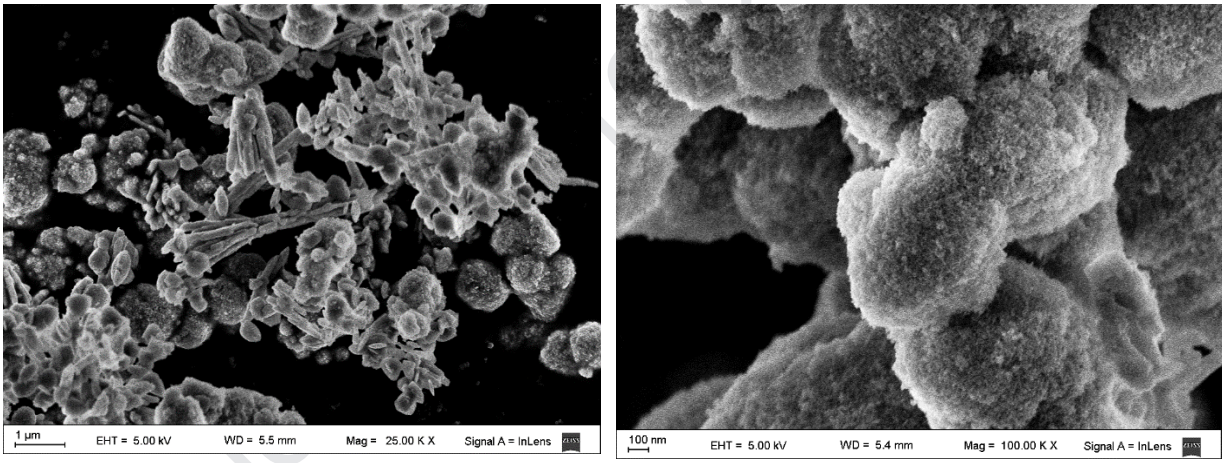

(b) CeO_2 U21 **C3C411** 120 8 500.

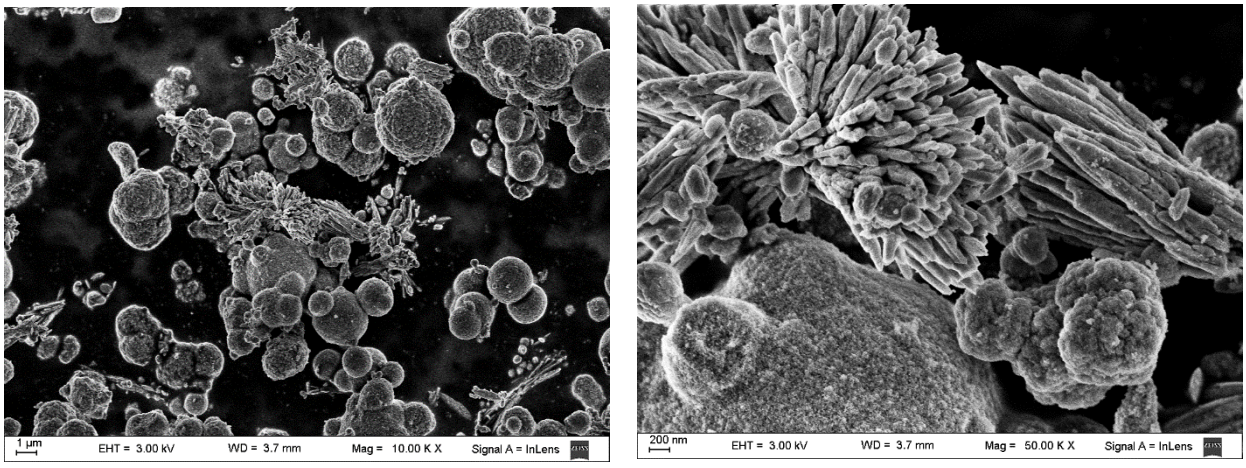

(c) CeO_2 U21 **C3C413** 120 8 500.

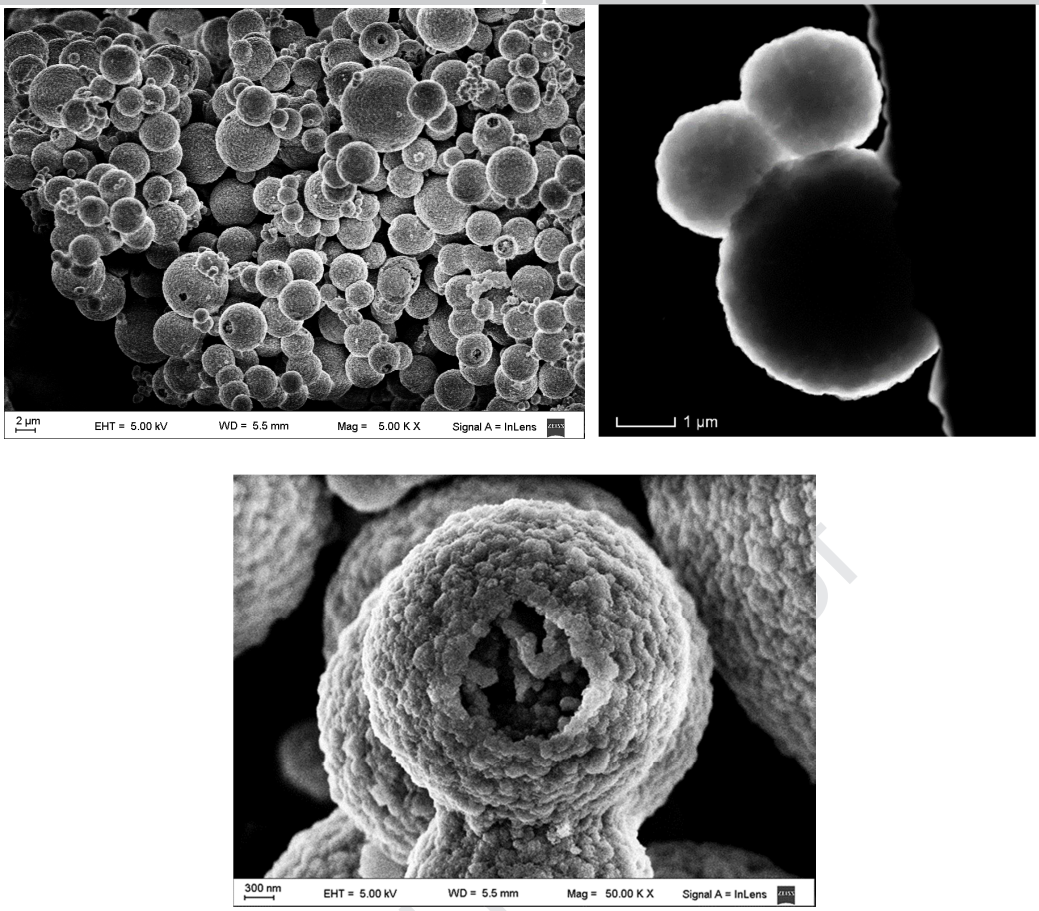

(d) CeO_2 U21 **C3C401** 120 8 500.

Figure 1. SEM and TEM micrographs of samples synthesized with different Ce^{3+}/Ce^{4+} molar ratios.

Table **2**. Initial and final values for the ionic strength of the reaction medium and their difference for samples synthesized with different Ce^{3+}/Ce^{4+} molar ratios in the initial solution.

Sample	$I_{initial}$ (M)	I_{final} (M)	ΔI (M)
CeO_2 U21 **C3C410**120 8 500	0.765	0.391	-0.374
CeO_2 U21 **C3C411** 120 8 500	0.574	0.606	0.033
CeO_2 U21 **C3C413** 120 8 500	0.478	0.686	0.208
CeO_2 U21 **C3C401** 120 8 500	0.382	0.766	0.383

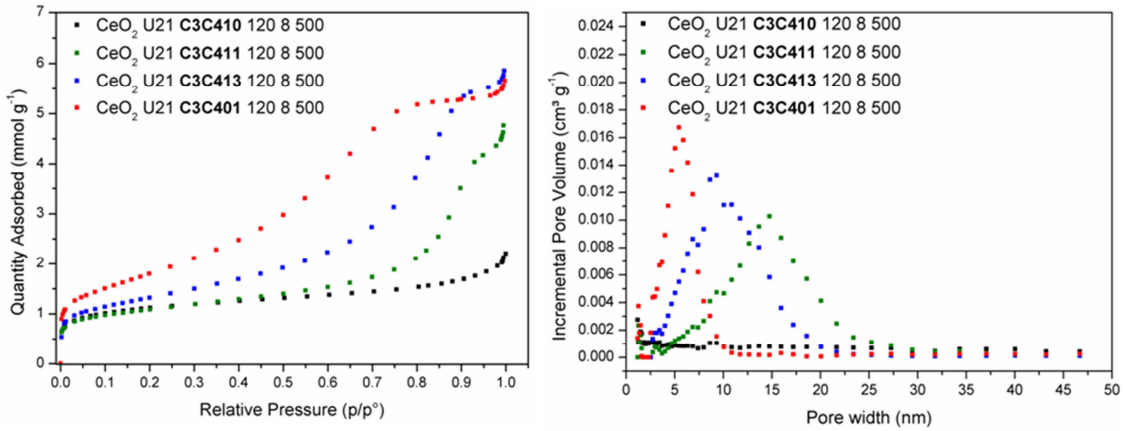

Figure **2.** N_2 adsorption isotherms and pore size distribution of samples synthesized with different Ce^{3+}/Ce^{4+} molar ratios.

In order to reveal the role of urea in the synthesis process, it was performed an extra synthesis without urea. Figures 3 and 4 present, respectively, XPD patterns and SEM micrographs for precursors CeO_2 U01 C3C410 120 8P and CeO_2 U21 C3C401 120 8P. It is confirmed that the presence of Ce^{4+} always leads to a fluorite structure. Spherical particles are only obtained if urea is used during the synthesis. If not, it takes place the hydrolysis of the strongly acidic $Ce(NO_3)_6^{2-}$, which is confirmed by the final pH value close to zero in the mother liquor, with no morphological control. Thus, not only the presence of Ce^{4+} but also urea are determining factors in the self-assembly process. At the temperature and pressure used in the hydrothermal process, urea decomposes increasing the pH to a value close to 9.25 which corresponds to that of the NH_3/NH_4^+ buffer and provides a high number of nucleation centers, a uniform and controlled nucleation rate, and a full precipitation reaction.

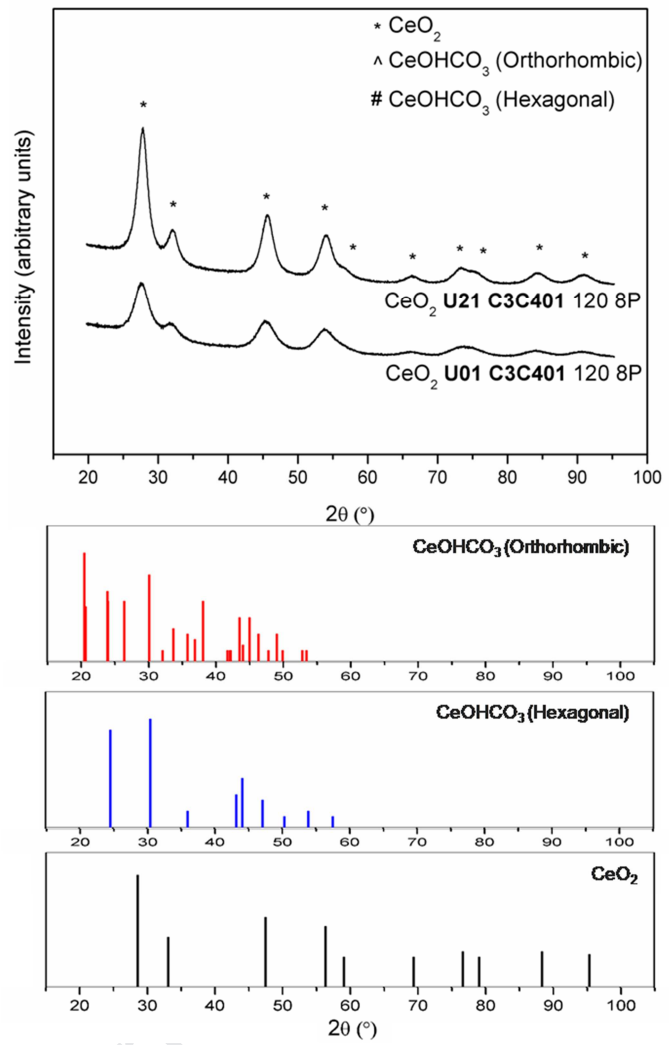

Figure 3. XPD patterns of the precursors CeO_2 **U21 C3C410** 120 8**P**, CeO_2 **U21 C3C401** 120 8**P** and CeO_2 **U01 C3C401** 120 8**P**.

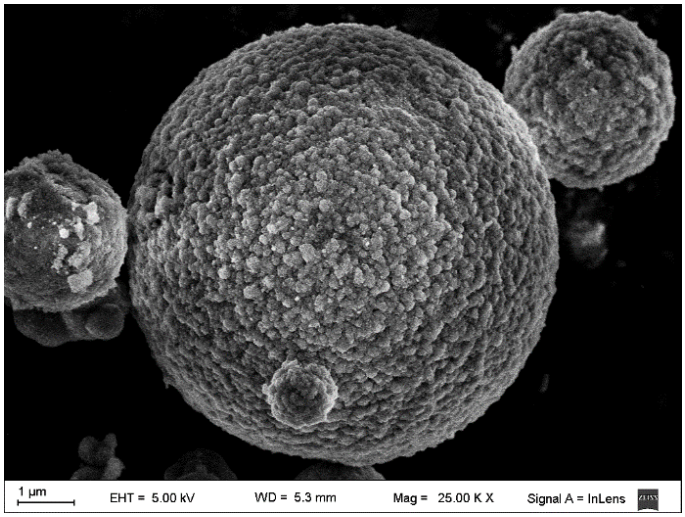

(a) CeO_2 **U21 C3C401** 120 8**P**.

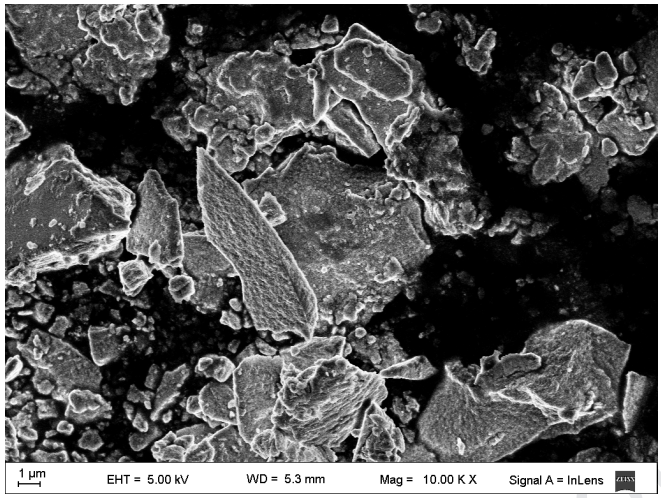

(**b**) CeO_2 **U01 C3C401** 120 8**P**.

Figure 4. SEM micrographs of precursors.

H_2-TPR profile of samples synthesized with different Ce^{3+} to Ce^{4+} molar ratios are presented in Figure **5(a)**. Profiles show two peaks, one at low temperatures (ca. 500 ºC) and the other one at high temperatures (ca. 700 ºC) usually assigned to the reduction of superficial and bulk Ce^{4+} species, respectively [**36**]. High-temperature peaks are similar while the influence of morphology is observed in the low-temperature reduction peaks. It is important to notice that despite the differences in specific surface area values, samples CeO_2 U21 **C3C413** 120 8 500 and CeO_2 U21 **C3C411** 120 8 500 have a similar percentage of reduction: 39% and 43%, respectively. Besides, the H_2-TPR profile for sample CeO_2 U21 **C3C401** 120 8 500 shows a negative peak in the 550-700 °C region. Laachir et al. [**37**] and Zotin et al. [**38**] have observed, **in CeO_2 with a very high specific surface area, the same lowering of the first TPR-peak area and the presence of the negative peak, assigning it to the desorption of gases strongly adsorbed on the surface, probably CO_2. Figure 5 (b) presents the H_2-TPRs of sample CeO_2 U21 C3C401 120 8 500 submitted to two different degassing pre-treatments: i) degassing at 300 °C for 30 minutes; ii) degassing at 450 °C for 30 minutes. In the case ii) the area of the negative peak was reduced and there was a corresponding increase in the area of the first TPR-peak, confirming the above-mentioned observations of other researchers [37,**

38]. These results justify the similarities observed in the first TPR peak of samples CeO_2 U21 C3C410 120 8 500 and CeO_2 U21 C3C401 120 8 500.

In summary, it is possible to say that the presence of Ce^{4+} and urea in the initial solution is crucial to gain control of the morphology, high specific surface area, high pore volume and pores in the mesopore region, with a strong effect on the TPR profile.

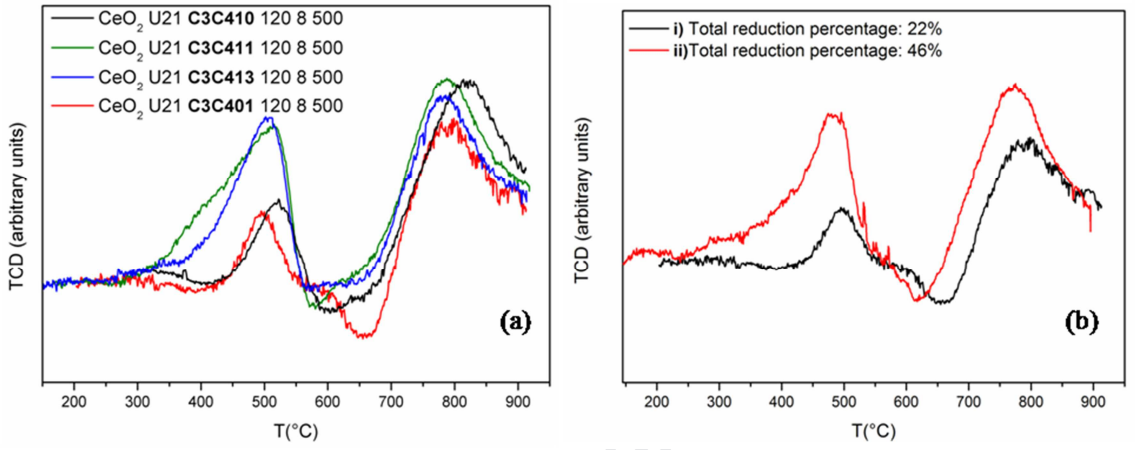

Figure 5.(a) H_2-TPR profile of samples synthesized with different Ce^{3+}/Ce^{4+} molar ratios. (b) H_2-TPR profile of sample CeO_2 U21 **C3C401 500 and degassed for 30 minutes i) at 300 °C and ii) at 450 ºC.**

Effect of Urea to Cation molar ratio in the initial solution

Figure **6** presents XPD patterns for samples obtained with different urea to cations molar ratios (U/C). In all cases, the Ce^{3+}/Ce^{4+} molar ratio is 1/0 and calcination temperature is 500 °C. It can be observed that all samples have the fluorite structure of pure CeO_2, with a face-centered cubic unit cell and $Fm\bar{3}m$ space group. Table **3** summarizes the main results obtained from Rietveld refinement and characterization techniques. Lattice parameters are slightly larger than the accepted for pure CeO_2 (a = 0.5413 nm, JCPDS 34-0394) possibly due to the presence of Ce^{3+} and oxygen vacancies. Crystallite sizes are in the nanometric range and lattice strain is very low and tends to decrease as the U/C ratio increases. SEM and TEM micrographs, as well as some Electron Diffraction (ED) patterns, are presented in Figure **7**. The morphology is strongly influenced by the U/C ratio. With U/C equal to 1/1 (Figure **7 (a1)** and **(a2)**) shuttle-like particles in the micrometer range are obtained. These big particles are polycrystalline with no ordered

aggregation of the crystallites **(see ED pattern presented in Figure 7 (a3))**. **As mentioned in the previous section, the decomposition of urea controls the pH and the nucleation rate.**

With an U/C molar ratio of 1/1, the final pH is 7 and shuttle-like particles are observed (see Figure 7 (a)). It is important to note that, of all the experiments performed, only in this case turbidity was observed when adding NaOH to the mother liquor, indicating the presence of unreacted Ce^{3+} species. Then, nucleation centers are not enough for complete precipitation.

With the increase in the U/C molar ratio to 2/1, the reaction is complete, with a final pH close to 9.25. As can be seen in Figure 7 (b), the process proceeds to an intermediate step in the hierarchical sequence and dumbbell-type morphologies are observed.

Finally, with an U/C molar ratio of 4/1, the excess of urea favors the speed of nucleation over the growth of the seeds, hindering the evolution of the self-assembly sequence (see Figure 7 (c)).

XPD patterns of precursors (see Figure S3) show the presence of $CeOHCO_3$ with orthorhombic structure (JCPDS No. 41-0013). The precipitation process starts with the strong hydration of Ce^{3+} that precipitates with the carbonate anions (CO_3^{2-}) provided by the decomposition of urea, as shuttle-shaped particles of $CeOHCO_3$ [21]. As U/C molar ratio increases, these shuttles evolve to dumbbell-like particles [28, 29]. No spheres were observed but other authors reported the synthesis of polycrystalline sphere-like structures with U/C ratios as high as 12 [17] and 67 [22]. It is worth to mention that these authors did not describe self-assembly mechanisms.

From the characterization results presented in Table 3, it is possible to say that U/C molar ratio has a mild effect on textural properties and reducibility. The pore size distribution is in the mesopore region with maxima in the 6-9 nm range and some porosity in the macropore region with maxima shifting to larger sizes as U/C increases (see Figure 8).

Table 3. Lattice parameter, lattice strain and crystallite size obtained from Rietveld refinement, total percentage of reduction obtained from H_2-TPR, BET specific surface area, total pore volume, and percentage of micropores volume of samples synthesized with different urea to cation molar ratios.

Sample	a [nm]	ε	D_V^{WH} [nm]	Percentage of Reduction (%)	S_{BET} [$m^2.g^{-1}$]	Total pore Volume [$cm^3.g^{-1}$]	Micropore to Total pore volume (%)
CeO_2 **U11** C3C410 120 8 500	0.5414(4)	$2.5\ 10^{-3}$	18	33	86	0.056	66
CeO_2 **U21** C3C410 120 8 500	0.5413(7)	$2.1\ 10^{-3}$	15	27	89	0.070	50
CeO_2 **U41** C3C410 120 8 500	0.5414(1)	$2.0\ 10^{-3}$	16	38	81	0.072	47

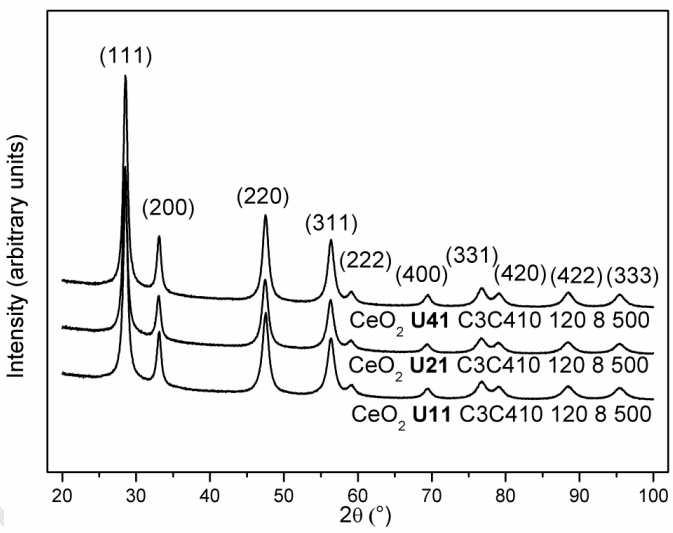

Figure 6. XPD patterns of samples synthesized with increasing urea to cation molar ratio.

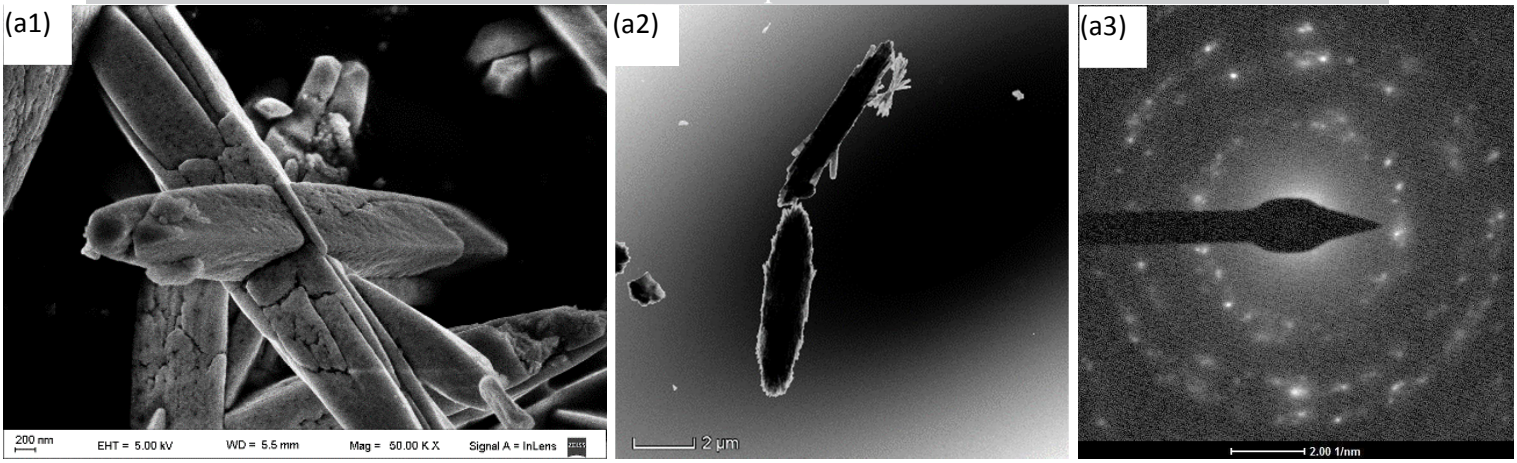

(a) CeO_2 **U11** C3C410 120 8 500.

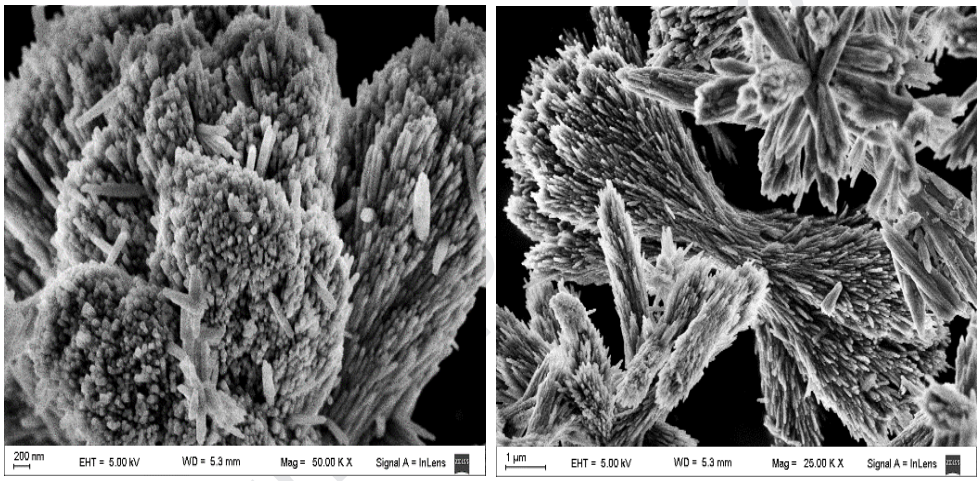

(b) CeO_2 **U21** C3C410 120 8 500.

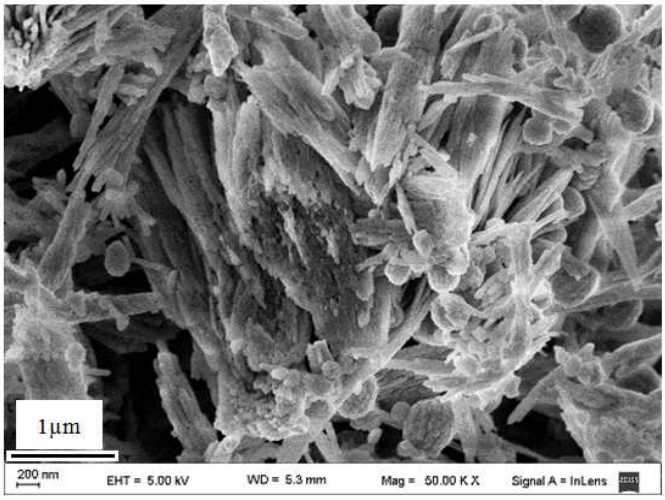

(c) CeO_2 **U41** C3C410 120 8 500.

Figure 7. SEM and TEM micrographs of samples synthesized with different urea to cation molar ratios.

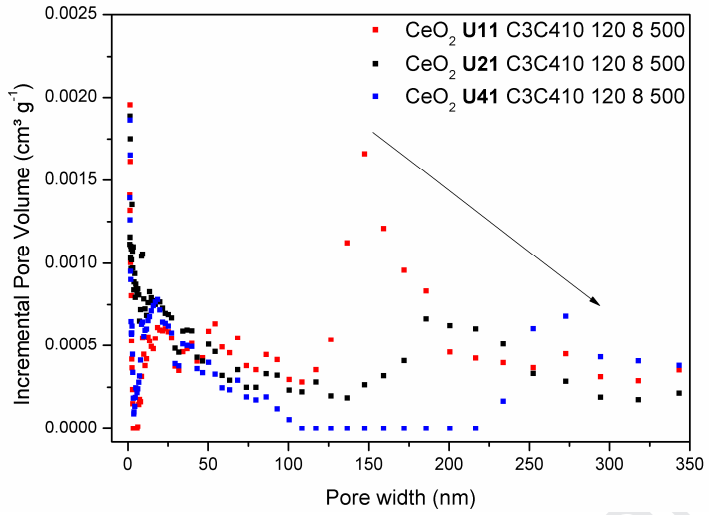

Figure 8. Pore size distribution of samples synthesized with different urea to cation molar ratios.

Effect of Reaction Temperature

For these experiments, samples were synthesized with a C3/C4 molar ratio equal to 1/0. The increase in the reaction temperature increases the nucleation rate. It takes place rapid precipitation of crystallites that agglomerate in shuttles, which evolve into dumbbells and spheres, highlighting the hierarchical self-assembly process (Figure S4). The increase in the reaction temperature produces a decrease in the dielectric constant of the water [4]. Therefore, strongly charged Ce^{3+} ions are hindered in their approach to growing nuclei, which provides more time for the self-assembly nucleation process to progress in its stages. The XPD results of the precursors confirm the presence of $CeOHCO_3$ with both orthorhombic and hexagonal structures, with an increase in the proportion of the hexagonal phase. At 150 °C and 180 °C, it is observed the appearance of a small amount of the fluorite phase (Figure S4). Concurrently, the presence of octahedral particles is observed in the SEM micrographs (Figures S4 and S5).

Structural, textural and redox properties do not show a clear influence of the reaction temperature (Table S1). Only the crystallite size clearly increases with its increment, and pore size distributions are in the 5.9-7.5 nm range.

Effect of reaction time

For these experiments, samples were synthesized with a C3/C4 molar ratio of 1/0. The precursors obtained with different reaction times have XPD patterns corresponding to the orthorhombic structure of $CeOHCO_3$ (Figure S6). For reaction times above 16 hours, a very small amount of CeO_2 appears probably due to the decomposition of $CeOHCO_3$ [21]. SEM micrographs showed in Figure S7 present morphologies corresponding to the self-assembly process already proposed in previous sections, but a detrimental effect is observed with the increase in reaction time.

Related to textural properties and reducibility it is clear, from results presented in Table S2, that BET specific surface area decreases and the reduction percentage increases with the increment in reaction time.

Conclusions

In this work, we report a comprehensive evaluation of a clean, extremely low waste, and green hydrothermal method to synthesize CeO_2. Our main conclusion is that it is possible to achieve high morphological control without using common templates, like surfactants or organic polymers, which generate hazardous effluents [39, 40, 41].

The present study shows the impact of the synthesis parameters of the hydrothermal method, Ce^{3+}/Ce^{4+} and urea to cation (U/C) molar ratios, reaction temperature and reaction time, on the properties of the obtained CeO_2 nanopowders. The results show that the presence of Ce^{4+} in the initial solution is crucial because it influences the precursor to get fluorite structures and is determinant to obtain non-hollow **spherical particles**, high specific surface area, high pore volume, and high reduction percentage. The urea to cation molar ratio controls the nucleation process and the morphology of the obtained particles, which evolve from shuttles to dumbbells and spheres as the ratio increases. The increase of urea in the starting solution results in a more crystalline precursor and demonstrated to be crucial to obtain the self-

assembly sequence. If only Ce^{3+} is present, $CeOHCO_3$ is obtained in the precursor and typical shuttle-like particles are obtained.

SEM results suggest the existence of a shuttle-dumbbell-sphere sequence [**28, 29**], which**, to** the best of our knowledge**, was** never reported without the aid of a template or structure-directing agent [**30, 31**]. It is worth to mention that the precursor samples morphology remains unchanged after calcination at 500 ºC. Hence, the morphologies here obtained and the variations on the applied conditions provide strong evidence of a hierarchical, template-free, sequential self-assembly process. The increase in ionic strength due to the different precursor salts used and the decrease of the dielectric constant, which is very important in hydrothermal conditions, seem to destabilize the reaction medium and induce the completion of the self-assembly sequence.

The increment in **reaction temperature** improves crystallinity **and has a strong influence on the morphology but has no effect** on the specific surface area, total pore volume and percentage of micropores.

The increment of the reaction time decreases the BET specific surface area and increases the reduction percentage.

Acknowledgments

The authors thank CONICET for the PhD Scholarship of Ing. Suarez Anzorena, ANPCyT for the financial support PICT 2013 N° 1587 and PICT 2016 N° 1921.

The authors offer special thanks to Dr. Alberto Caneiro for his relevant support during TEM studies.

References

[1] Z. Li, X. Niu, Z. Lin, N. Wang, H. Shen, W. Liu, K. Sun, Y. Q. Fu, Z. Wang, Hydrothermal synthesized CeO_2 nanowires for H_2S sensing at room temperature, J. Alloys Compd. 682 (2016), 647-653. https://doi.org/10.1016/j.jallcom.2016.04.311

[2] T. Montini, M. Melchionna, M. Monai, P. Fornasiero, Fundamentals and Catalytic Applications of CeO_2-Based Materials, Chem. Rev. 116 (2016), 5987−6041. https://doi.org/10.1021/acs.chemrev.5b00603

[3] M. Yashima "Catalysis by Ceria Related Materials", Chapter 1, A. Trovarelli, P. Fornasiero, (Eds), Second Edition, Imperial College Press, London, England (2013).

[4] S. Feng, G. Li, "Modern Inorganic Synthetic Chemistry", eds. R. Xu, W. Pang, Q. Huo, Elsevier, Chapter 4, 2011, 63-65.

[5] Q. Yuan, H. Duan, L. Li, L. Sun, Y. Zhang, C. Yan, Controlled synthesis and assembly of ceria-based nanomaterials; Journal of Colloid and Interfaces Science, 335, (2009) 151-167. http://doi:10.1016/j.jcis.2009.04.007

[6] S. Gnanam, V. Rajendran, Influence of Various Surfactants on Size, Morphology, and Optical Properties of CeO_2 Nanostructures via Facile Hydrothermal Route; Journal of Nanoparticles, 2013, (2013) Article ID 839391, 6 pages. http://dx.doi.org/10.1155/2013/839391

[7] A.I.Y. Tok, F.Y.C. Boey, Z. Dong, X.L. Sun, Hydrothermal synthesis of CeO2 nano-particles; Journal of Materials Processing Technology, 190, (2007) 217-222. https://doi.org/10.1016/j.jmatprotec.2007.02.042

[8] N. Wu, E. Shi, Y. Zheng, W. Li, Effect of pH of Medium on Hydrothermal Synthesis of Nanocrystalline Cerium(IV) Oxide Powders; J. Am. Ceram. Soc. 85, 10, (2002) 2462-2468. https://doi.org/10.1111/j.1151-2916.2002.tb00481.x

[9] T. Taniguchi, K. Katsumata, S. Omata, K. Okada, N. Matsushita, Tuning Growth Modes of Ceria-Based Nanocubes by a Hydrothermal Method; Cryst. Growth Des. 11 (2011) 3754–3760.http://dx.doi.org/10.1021/cg101585b

[**10**] W. Wang, R. Guo, W. Pan, G. Xu, Low temperature catalytic oxidation of NO different-shaped CeO_2, Journal of rare Earths 36 (2018), 588-593. https://doi.org/10.1016/j.jre.2017.10.002

[**11**] A. K. P. Mann, Z. Wu, F. C. Calaza, S. H. Overbury, Adsorption and Reaction of Acetaldehyde on Shape-Controlled CeO_2 Nanocrystals: Elucidation of Structure-Function Relationships, American Chemical Society Catalysis (2014) 4, 2437-2448. https://doi.org/10.1021/cs500611g

[**12**] P.Stelmachowski, K. Ciura, P. Indyka, A. Kotarba, Facile synthesis of ordered CeO_2 nanorod assemblies: Morphology and reactivity, Materials Chemistry and Physics 201 (2017), 139-146. https://doi.org/10.1016/j.matchemphys.2017.08.038

[**13**] Z. Yang, Y. Yang, H. Liang, L. Liu, Hydrothermal synthesis of monodisperse CeO_2nanocubes, Materials Letters 63 (2009), 1774-1777. https://doi.org/10.1016/j.matlet.2009.05.034

[**14**] F. Meng, J. Gong, Z. Fan, H. Li, J. Yuan, Hydrothermal synthesis and mechanism of triangular prism-like monocrystalline CeO_2 nanotubes via a facile template-free hydrothermal route, Ceramics International 42 (2016), 4700-4708. https://doi.org/10.1016/j.ceramint.2015.11.123

[**15**] F. Hu, J. Chen, Y. Peng, H. Song, K. Li, J. Li, Novel nanowire self-assembled hierarchical CeO_2 microspheres for low temperature toluene catalytic combustion, Chemical Engineering Journal 331 (2018), 425-434. https://doi.org/10.1016/j.cej.2017.08.110

[**16**] Z. Guo, F. Du, Z. Cui, Hydrothermal synthesis of single-crystalline $CeCO_3OH$ flower-like nanostructures and their thermal conversion to CeO_2, Materials Chemistry and Physics 113 (2009), 53-56. https://doi.org/10.1016/j.matchemphys.2008.07.029

[**17**] H. Li, G. Lu, Q. Dai, Y. Wang, Y. Guo, Y. Guo, Hierarchical organization and catalytic activity of high-surface-area mesoporous ceria microspheres prepared via hydrothermal routes, Applied Materials and Interfaces 2 (2010), 838-846. DOI: 10.1021/am900829y.

[**18**] T. Guo, J. Du, J. Wu, J. Li, Palladium catalyst supported on stair-like microstructural CeO_2 provides enhanced activity and stability for low-concentration methane oxidation, Applied Catalysis A: General 524 (2016), 237-242. https://doi.org/10.1016/j.apcata.2016.06.040

[**19**] K. Nakagawa, T. Oshima, Y. Tezuka, M. Katayama, M. Katoh, S. Sugiyama, Morphological effects of CeO_2 nanostructures for catalytic soot combustion of CuO/CeO_2, Catalysis Today 246 (2015), 67-71. https://doi.org/10.1016/j.cattod.2014.08.005

[**20**] H. Li, F. Meng, J. Gong, Z. Fan, R. Qin, Structural, morphological and optical properties of shuttle-like CeO_2 synthesized by a facile hydrothermal method, Journal of Alloys and Compounds 722 (2017), 489-498. https://doi.org/10.1016/j.jallcom.2017.06.156

[**21**] G. Shen, Q. Wang, Z. Wang, Y. Chen, Hydrothermal synthesis of CeO_2 nano-octahedrons, Materials Letters 65 (2011), 1211-1214.https://doi.org/10.1016/j.matlet.2011.01.057

[**22**] N. Ta, M. Zhang, J. Li, H. Li, Y. Li, W. Shen, Facile Synthesis of CeO_2 Nanospheres, Chinese Journal of Catalysis 29 (11) (2008), 1070-1072. https://doi.org/10.1016/S1872-2067(09),60002-4

[**23**] J. Gong, F. Meng, Z. Fan, H. Li, Z. Du, Template-free controlled hydrothermal synthesis for monodisperse flowerlike porous CeO_2 microspheres and their superior catalytic reduction of NO with NH_3, Journal of Alloys and Compounds 690 (2017), 677-687. https://doi.org/10.1016/j.jallcom.2016.08.183

[**24**] H. Liu, H. Liu, Preparing micro/nano dumbbell-shaped CeO_2 for high performance electrode materials, Journal of Alloys and Compounds 681 (2016), 342-349. https://doi.org/10.1016/j.jallcom.2016.04.207

[**25**] A.I.Y. Tok, F.Y.C. Boey, Z. Dong, X. L. Sun, Hydrothermal synthesis of CeO_2nano-particles, Journal of Materials Processing Technology 190 (2007), 217-222. https://doi.org/10.1016/j.jmatprotec.2007.02.042

[**26**] P.J. Geiger, The use of p-dimethylaminobenzaldehyde for the microdetermination of urea in urine, Microchem. J. 13 (1968), 481-490. https://doi.org/10.1016/0026-265X(68)90115-X

[**27**] R. Guinebretiere, "X-ray Diffraction by Polycrystalline Materials",ISTE Ltd, Great Britain, 2007.

[**28**] S. Yu, H. Cöelfen, "Nanoparticle Assemblies and Superstructures"**,** Chapter 11, N. A. Kotov (Ed), Taylor & Francis Group, CRC Press (2006).

[**29**] H. Cöelfen, M. Antonietti, "Mesocrystals and Nonclassical Crystallization", Chapter 11, John Wiley and Sons, Chichester, England (2008).

[**30**]Z. Gu, T. Zhai, B. Gao, G. Zhang, D. Ke, Y. Ma, J. Yao,Controlled Hydrothermal Synthesis of Nickel PhosphiteNanocrystals with Hierarchical Superstructures, Cryst. GrowthDes. Vol. 7, No. 4, (2007), 825-830. https://doi.org/10.1021/cg060774c

[**31**]G. Chen, B. Dneg, G. Cai, T. Zhang, W. Dong, W. Zhang, A. Xu, The Fractal Splitting Growth of Sb_2S_3 and Sb_2Se_3 Hierarchical Nanostructures, J. Phys. Chem. C, 112, (2008) 672-679. https://doi.org/10.1021/jp076883z

[**32**] S. Cotton, “Lanthanide and Actinide Chemistry”, Chapter 4, John Wiley and Sons, Chichester, England (2006).

[**33**] S. Cotton, J. M. Harrowfield, “Rare Earth fundamentals and applications”, Chapter 3, D. A. Atwood (Ed), John Wiley and Sons, Chichester, England (2012).

[**34**] A. Bumajdad, J. Eastoe, A. Mathew, Cerium oxide nanoparticles prepared in self-assembled systems, Adv. Colloid Interface Sci. 147–148 (2009), 56-66. https://doi.org/10.1016/j.cis.2008.10.004

[**35**] J. Eastoe, M. Hollamby, L. Hudson, Recent advances in nanoparticle synthesis with reversed micelles, Adv. Colloid Interface Sci. 128–130 (2006), 5-15.https://doi.org/10.1016/j.cis.2006.11.009

[**36**] A. Trovarelli, Catalytic Properties of Ceria and CeO_2-Containing Materials, Catal. Rev. Sci. Eng. 38 (4) (1996), 439-520.http://dx.doi.org/10.1080/01614949608006464

[**37**] A. Laachir, V. Perrichon, A. Badri, J. Lamotte, E. Catherine, J. C. Lavalley, J. E. Fallah, L. Hilaire, F. le Normand, E. Quéméré, G. N. Sauvion, O. Touret, Reduction of CeO_2 by Hydrogen, J. Chem. Soc. Faraday Trans. 87 (10) (1991), 1601-1609.doi.10.1039/FT9918701601

[**38**] F. M. Z. Zotin, L. Tournayan, J. Varloud, V. Perrichon, R. Fréty, Temperature-programmed reduction: limitation of the technique for determining the extent of reduction of either pure ceria or ceria modified additives, Appl. Catal. A Gen. 98 (1993), 99-114. https://doi.org/10.1016/0926-860X(93)85028-N

[**39**] J. Dahl, B. Maddux, J. Hutchison, Toward greener nanosynthesis, Chem. Rev.107, (2007). https://doi.org/10.1021/cr050943k

[**40**] S. Sharma, A. Mudhoo, W. Zhang; Chapter 1, Green Chemistry for Environmental Sustainability, S. Sharma, A. Mudhoo (Eds), Taylor & Francis Group, CRC Press (2011).

[**41**] D. Dirk, M, Peter; "Green Chemistry, Environmentally Benign Approaches", Chapter 1, M. Kidwai, N. Mishra (Eds), InTech, Croatia (2012).

Declaration of interests

☒ The authors declare that they have no known competing financial interests or personal relationships that could have appeared to influence the work reported in this paper.

☐The authors declare the following financial interests/personal relationships which may be considered as potential competing interests: